ADVANCED ELECTRONIC MATERIALS
www.advelectronicmat.de

Solution Processable Pentafluorophenyl End-Capped Dithienothiophene Organic Semiconductors for Hole-Transporting Organic Field Effect Transistors

Arulmozhi Velusamy, Yung-Chi Yang, Chia-Chi Lin, Shakil N. Afraj, Kexing Jiang, Peng-Sheng Chen, Shueh-Lin Yau, Itaru Osaka, Shih-Huang Tung, Ming-Chou Chen, and Cheng-Liang Liu**

Two solution-processable organic semiconductors, DFPT-DTTR (1) and DFPbT-DTTR (2), composed of pentafluorophenyl (FP) end-capped 3,5-dialkyl dithienothiophene (DTTR) core with thiophene (T) or bithiophene (bT) as π-bridged spacers are developed and investigated for their optical, electrochemical, microstructural, and electrical properties. With more conjugated bithiophene units, compound 2 exhibits a red-shifted UV–vis absorption band and upshifted HOMO/downshifted LUMO energy levels. According to the density functional theory, compound 2 features a more twisted molecular structure due to the intrinsic non-coplanar blocks in the π-backbones. Compound 1-based organic field effect transistors exhibit efficient hole transport with mobility up to 0.48 $cm^2 V^{-1} s^{-1}$. This is one of the high mobility organic semiconductors exhibiting p-channel characteristics based on solution-processable small molecular FP end-capped fused/oligothiophenes. With large and interconnected crystalline morphologies, decreased π–π stacking distance, and less steric hindrance, compound 1 exhibits two orders of magnitude higher mobility than the more distorted 2, which exhibits lower hole mobility of 1.82×10^{-3} $cm^2 V^{-1} s^{-1}$.

A. Velusamy, S. N. Afraj, P.-S. Chen, S.-L. Yau, M.-C. Chen
Department of Chemistry
National Central University
Taoyuan 32001, Taiwan
E-mail: mcchen@ncu.edu.tw

Y.-C. Yang, C.-C. Lin, K. Jiang
Department of Chemical and Materials Engineering
National Central University
Taoyuan 32001, Taiwan

C.-C. Lin, I. Osaka
Applied Chemistry Program
Graduate School of Advance Science and Engineering
Hiroshima University
Higashi-Hiroshima
Hiroshima 739–8527, Japan

S.-H. Tung
Institute of Polymer Science and Engineering
National Taiwan University
Taipei 10617, Taiwan

C.-L. Liu
Department of Materials Science and Engineering
National Taiwan University
Taipei 10617, Taiwan
E-mail: liucl@ntu.edu.tw

The ORCID identification number(s) for the author(s) of this article can be found under https://doi.org/10.1002/aelm.202100648.

DOI: 10.1002/aelm.202100648

1. Introduction

The design, synthesis, and structural characterization of new organic π-conjugated materials are important aspects in the scientific and technological development of next-generation optoelectronic devices.[1] Due to their diverse applications as electro-active materials, organic semiconductors have gained attention for the development of low-cost, large-area printable, and flexible electronic devices such as organic field effect transistors (OFETs), organic light-emitting diodes (OLEDs), and organic photovoltaics (OPVs).[2–13] In contrast to the traditional inorganic materials, organic semiconductors are promising essential components for future optoelectronic devices.[14–15] The well-known acene-based organic semiconductors (OSCs),[16–18] such as pentacenes[19–20] have attracted much attention because of their excellent charge transport properties. However, the lower solubilities and chemical stabilities of acene-based OSCs critically limited their applications in optoelectronic devices.[21–22] The low stability of acene-based OSCs mainly suffers from oxidation in the presence of light and oxygen.[23] To overcome these disadvantages, fused thiophenes and their derivatives have been widely explored as alternative materials because of their efficient charge carrier transport rising from the planar backbone structure, extensive conjugation, strong π–π stacking/intermolecular interactions in the solid state, and excellent ambient stability.[22,24–32] It is anticipated that modification of fused thiophenes will play a vital role in the next-generation organic semiconductors for high-performance and air-stable devices.[25,33–35]

As shown in **Figures 1** and **2**, most of the reported fused thiophene based small molecular organic semiconductors (A,[36] B,[37] D,[38] E,[31] F,[39] G,[40] and N–S[24–25,41–44]) have been fabricated via vacuum deposition due to their low solubility. Strategies for the development of high-performance, solution-processable, environmentally stable organic semiconductors include carefully placing solubilizing substituents onto the core to enhance solubility without disrupting the backbone π-conjugation for close molecular arrangement.[45–49] To date, only a few solution-processable p-type small molecular fused thiophenes based organic semiconductors (C,[50] H,[21] I,[51] and J[52])

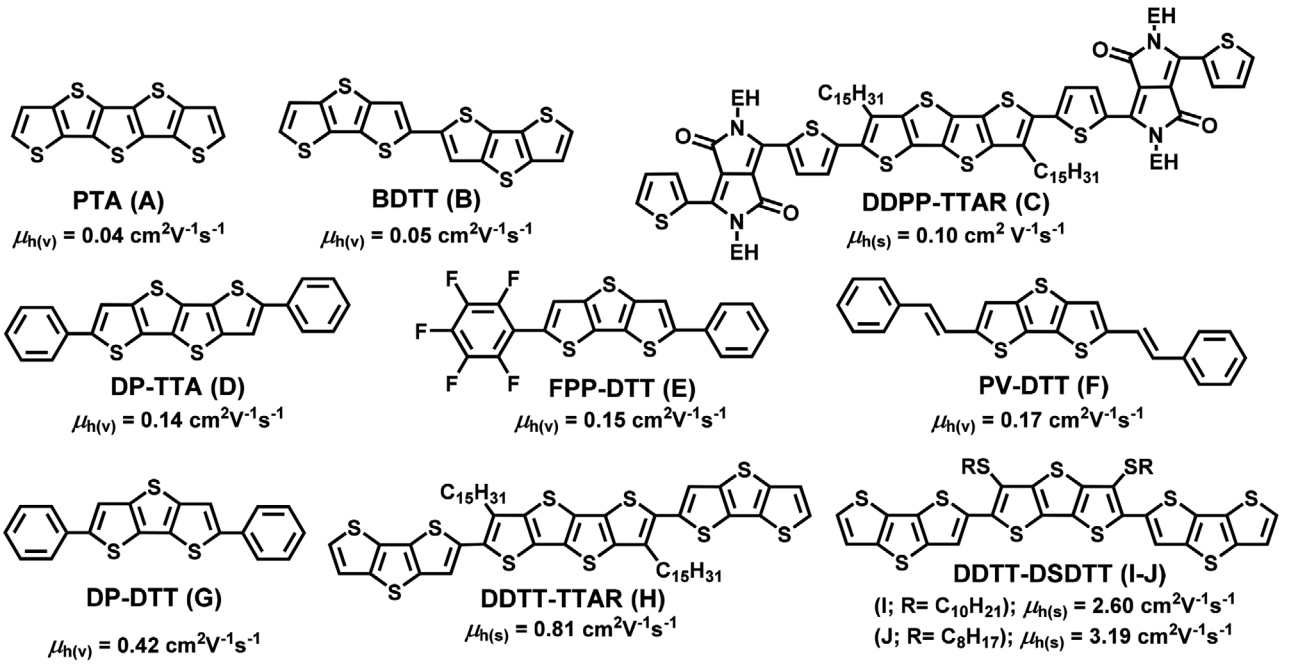

Figure 1. Examples of p-type fused thiophenes-based organic semiconductors and their OFET performances. The symbol (μ_h) denotes hole mobilitity, while (*v*) and (s) denote semiconductor films obtained from the vacuum process and solution-shearing process respectively.

have been reported with decent transport performance. For example, *β*-alkylated tetrathienoacene (TTAR)-based solution-processable small molecules DDPP-TTAR (C)[50] and DDTT-TTAR (H)[21] exhibited hole mobilities of 0.1 and 0.81 cm^2 V^{-1} s^{-1} in OFETs, respectively. More recently, a new strategy for the development of highly planar *π*-conjugated semiconductors for OFETs was achieved. Noncovalent confirmational locks between the heteroatom on the *β*-position and heteroatom atom on the neighboring aromatic units offered high-performance organic semiconductors.[51–54] As shown in Figure 1, solution-processable 3,5-dithioalkyl dithienothiophene (DSDTT)-based small molecular semiconductors I and J achieved record high hole mobilities of 2.60 and 3.19 cm^2 V^{-1} s^{-1}, respectively.[51–52]

One approach for the development of new organic semiconductors with decent electron transport is to functionalize the conjugated central core with strong electron withdrawing substituents.[24,35,41,47–48,55] In particular, Marks and co-workers reported the first fluoroarene-modified oligothiophene semiconductors.[56] The perfluorophenyl (FP) end-capped oligothiophene based semiconductors (compound K) was developed with electron mobility of 0.08 cm^2 V^{-1} s^{-1}. Later, as shown in Figure 2, electronegative perfluoroalkyl or FP end-capped fused/oligo-thiophenes were explored[57–58] and DFHCO-4T (L) based OFET device achieved the highest electron mobility up to 2.0 cm^2 V^{-1} s^{-1}.[59] In contrast, FP-capped organic semiconductors, DFCO-4T (M),[57] FBB-DTT (N),[41] D(Ph$_F$CO)-BTBT (O),[43] DFP-DTT (P),[42] DFP-TTA (Q),[24] and DFPT-TTA (R)[25] exhibited relatively lower electron mobilities of 0.03–0.57 cm^2 V^{-1} s^{-1}. Interestingly, among these fused thiophenes based organic semiconductors, OFETs with longer conjugation on their fused central cores (e.g., from P to R) exhibit higher mobility. Nevertheless, very few FP end-capped organic semiconductors were reported with a hole or ambipolar characteristics. For example, asymmetric fused thiophene molecule FPP-DTT (E) exclusively recorded p-channel mobilities of 0.74 and 0.15 cm^2 V^{-1} s^{-1} for single crystal and thin film based OFET devices, respectively,[31] whereas, FP-capped DFPADT (S)-based OFETs exhibited ambipolar transport with mobilities of 0.048 and 6×10^{-4} cm^2 V^{-1} s^{-1} for hole and electron, respectively.[44]

Herein, to further search for new solution-processable fused thiophenes with higher charge transport characteristics, *β*-alkylated dithienothiophene (3,5-dialkyldithieno[3,2-*b*:2′,3′-*d*] thiophene; DTTR; R = $C_{11}H_{23}$) was explored as a central core, FP served as a capping end, and thiophene or bithiophene units were employed as *π*-spacers for conjugation extension. The regiochemistry of FP electron-withdrawing moieties with respect to the *π*-backbone plays a fundamental role in establishing the active semiconducting channel.[56] Thus, FP-served as end-capping unit due to the following criteria: i) electron-withdrawing perfluorophenyl substitution on electron-donating fused/oligo thiophene central core should lower LUMO energies for efficient charge transport,[60] and ii) combination of electron-rich and electron-deficient *π*-rings should favor close cofacial *π*–*π* stacking,[28,56] iii) nonbonded interactions between hydrogen and fluorine (F···H) will increase the *π*–*π* stacking, leading to the closer molecular arrangement and thus will enhance the device performance.[41] Hence, we developed two new solution-processable organic semiconductors, DFPT-DTTR (1) and DFPbT-DTTR (2), (as shown in **Scheme 1**), which exhibited solo hole carrier mobilities (μ_h) of 0.48 and 1.82×10^{-3} cm^2 V^{-1} s^{-1}, for 1 and 2, respectively. This is one of the high mobility OSCs exhibiting p-channel characteristics based on solution-processable small molecular FP end-capped fused/oligothiophenes. The material properties of these newly synthesized FP end-capped DTTR-based analogs, such as physical properties, HOMO–LUMO energies, and film microstructure, are discussed and the film growth conditions were shown to strongly influence the thin film transistor device response.

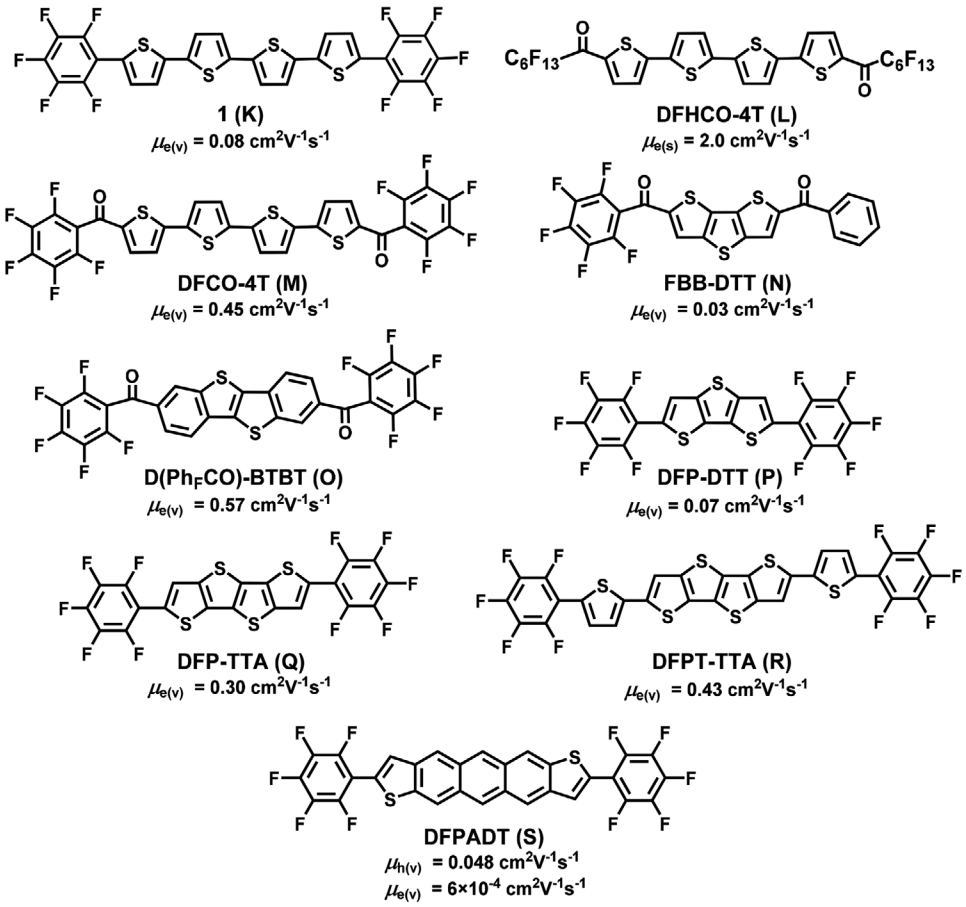

Figure 2. Examples of perfluoroalkyl or pentafluorophenyl end-capped fused/oligo thiophenes-based organic semiconductors and their OFET performances. The symbols (μ_e) and (μ_h) denotes electron and hole mobility, respectively, while (*v*) and (*s*) denote semiconductor films obtained from the vacuum process and solution-shearing process respectively.

2. Results and Discussion

The 3,5-dialkyldithieno[3,2-*b*:2′,3′-*d*]thiophene (DTTR; 3) central core was prepared according to the literature.[47] Dibromination of compound 3 with *n*-bromosuccinimide and Stille coupling with 2-tri-*n*-butylstannylthiophene yielded 2,6-di(thiophen-2-yl)-3,5-dialkyldithieno[3,2-b:2′,3′-d]thiophene (DT-DTTR; 4). The pentafluorophenyl end-capped DTTR derivatives were synthesized via a Pd-catalyzed Stille cross-coupling reaction, as shown in Scheme 1. First, the fused thiophenes (3 and 4) were di-deprotonated with *n*-BuLi, followed by stannylation using tri-*n*-butyltin chloride to yield the corresponding fused thiophene stannylates in situ. Then, Stille couplings were performed between the latter with 2-bromo-5-(perfluorophenyl) thiophene (FPT-Br; 5) to give the corresponding final products, DFPT-DTTR (1) and DFPbT-DTTR (2), yielding ≈55% and ≈67%,

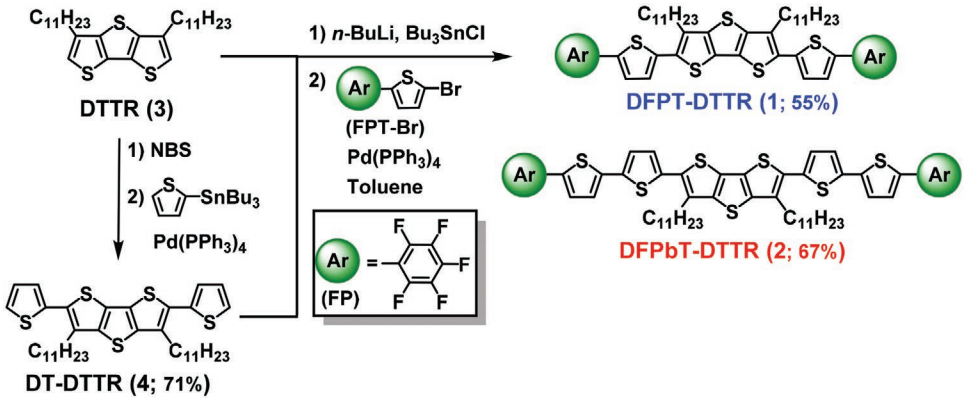

Scheme 1. Synthetic route to DTTR-based compounds (1 and 2).

Table 1. Thermal, optical, and electrochemical properties of DTTRs 1 and 2.

Compound	T_d [°C][a]	T_m[C][b]	λ_{max} (soln) [nm][c]	λ_{max} (film) [nm][d]	E_g [eV][e]	E_{ox} [V][f]	E_{HOMO} [eV][f]	E_{LUMO} [eV][g]
DFPT-DTTR (1)	384	169	411	510	2.33	1.16	−5.36	−3.03
DFPbT-DTTR (2)	358	165	440	540	2.11	1.03	−5.23	−3.12

[a]Decomposition temperatures were determined from TGA; [b]Melting temperatures were determined from DSC; [c]In *o*-$C_6H_4Cl_2$; [d]From solution-sheared films; [e]Calculated by using the optical absorption onset, $1240/\lambda_{onset}$; [f]By DPV in *o*-$C_6H_4Cl_2$ at 25 °C. All potentials are reported with reference to an Fc/Fc$^+$ internal standard (at +0.6 V). $E_{HOMO} = -(4.2 + E_{ox})$; [g]$E_{LUMO} = E_{HOMO} + \Delta E_g$.

respectively. The obtained newly synthesized compounds 1 and 2 were then purified by recrystallization and both exhibited adequate solubility in common organic solvents due to their long alkyl side chain substituents on the central core, which is the primary requirement for solution-processable OFET devices. These new DTTR derivatives were fully characterized by ^{1}H, ^{13}C and ^{19}F NMR and mass spectrometry. The synthetic procedure details and characterization data are provided (Scheme S1 and Figures S1–S5, Supporting Information). Thermal analyses of the new alkylated DTTR-based organic semiconductors were performed using differential scanning calorimetry (DSC; Figure S6, Supporting Information) and thermogravimetric analysis (TGA; Figure S7, Supporting Information), and the corresponding thermal data are summarized in **Table 1**. DSC scans revealed major endotherms at 169 and 165 °C for compounds 1 and 2, respectively, while the exothermic peak due to the crystallization was also found around 121 and 147 °C. TGA scans demonstrated high thermal stability with ≈5% weight loss temperature around 384 and 358 °C for compounds 1 and 2, respectively, indicating that the new FP end-capped DTTRs possess high thermal stability. The high thermal stable behavior of these two compounds with the presence of crystalline structures is beneficial for efficient charge transfer in OFETs application.

The optical absorption properties of two compounds were analyzed in solution (dichlorobenzene) and thin film. **Figure 3** shows the UV–vis absorption spectra, and the peak maximum (λ_{max}) and bandgap (E_g) extracted from the absorption onset are summarized in Table 1. In solution, both compounds 1 and 2 show similar spectral shapes with two absorption bands at λ_{max} of 411/440 and 342/337 nm, corresponding to 0–0 and 0–1 vibrational peaks, respectively. A clear red-shift from the solution to thin film state (*J*-aggregation like)[25] was observed because of the stronger intermolecular interactions between the molecules. The thin film of compound 2 exhibits several λ_{max} assigned to the typical vibronic progression of a π-conjugated fused heteroacene, with substantially red-shifted λ_{max} and onset values compared to compound 1, attributed to the presence of an additional electron-donating thiophene linker on each side of the DTTR core. As expected, the optical bandgap of compound 2 was estimated as 2.11 eV, which is considerably smaller than that of compound 1 (2.33 eV). Differential pulse voltammetry (DPV) was performed to characterize the energy level of the compounds using 0.1 M solution of tetrabutylammonium hexafluorophosphate ($TBAPF_6$) in a dry *o*-dichlorobenzene solvent with the addition of ferrocene (Fc/Fc$^+$) as internal standard. As shown in **Figure 4**a, the oxidation peaks (E_{ox}) of DTTRs 1 and 2 occur at 1.16 and 1.03 V, respectively, which evidences that the effect of more electron-donating bithiophene linkers makes the compound 2 more easily oxidized.

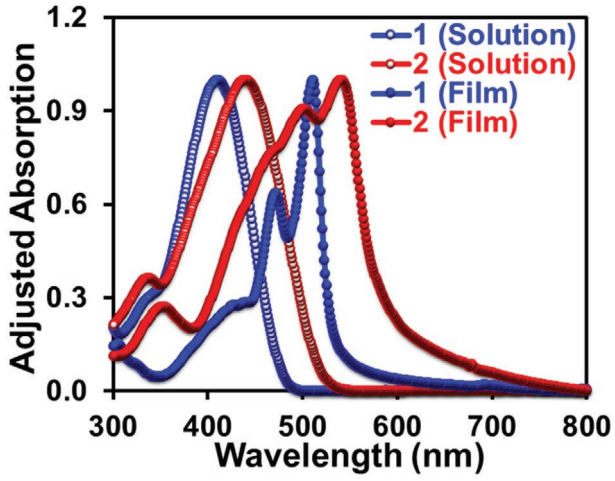

Figure 3. UV–vis absorption spectra of compound 1 and 2 in chlorobenzene solutions and as thin films.

The derived energies of the highest occupied molecular orbital (E_{HOMO}) of 1 and 2 are located around −5.36 and −5.23 eV, respectively, according to the equation: $E_{HOMO} = -(4.2 + E_{ox})$; assuming an internal standard Fc/Fc$^+$ oxidation at −4.8 eV.[48] The E_{HOMO} of compound 2 is higher than that determined for compound 1, which is consistent with the values obtained from the DFT theoretic calculation (vide infra). The energies of the lowest unoccupied molecular orbital (E_{LUMO}) are indirectly estimated by adding the previously measured optical bandgap to the E_{HOMO}. The E_{HOMO} and E_{LUMO} values for these two compounds are reported in Table 1 and Figure 4b provides a graphical comparison. The up-shifted HOMO and downshifted LUMO level of compound 2 compared to compound 1 originates from the additional electron-donating thiophene.[61] The lower electrochemically derived E_{HOMO} of these two new DTTRs, 1 (−5.36 eV) and 2 (−5.23 eV), compared to pentacene (−5.02 eV)[62] suggest that these newly developed fused thiophenes are environmentally stable. In addition, the energy gaps of 1 (2.33 eV) and 2 (2.11 eV) are larger than that of pentacene (2.09 eV).[62] The larger optical bandgaps imply that these compounds are not easily oxidized and have better stability in air. The photooxidative stability of DTTR derivatives was investigated by monitoring the maximum absorption (λ_{max}) values of 411 and 440 nm (for compound 1 and 2, respectively) in aerated *o*-dichlorobenzene solutions while exposing to white light (fluorescent lamp) at room temperature. This experiment was carried out over 10 days and the maximum absorption values are almost identical and a linear graph was obtained for

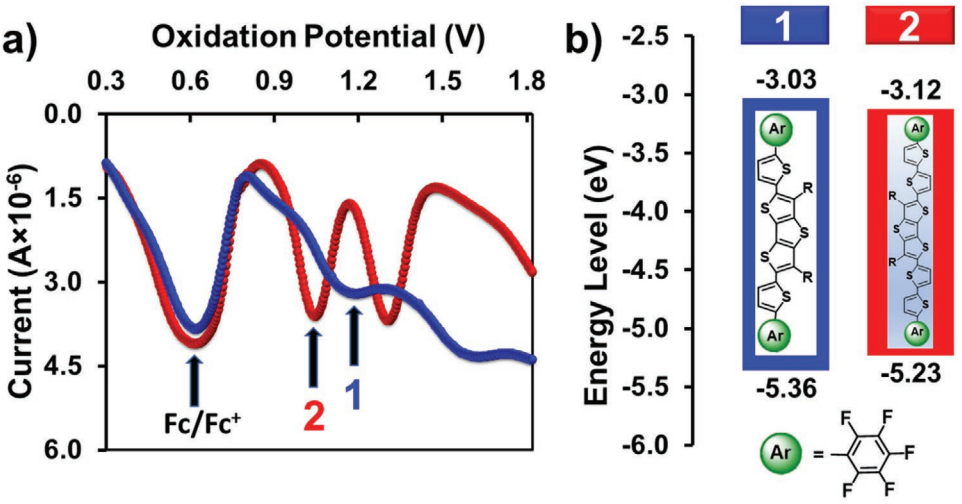

Figure 4. a) Oxidation potential curves (in *o*-dichlorobenzene). b) Energy level schematic diagram of DFPT-DTTR (1) and DFPbT-DTTR (2). All potentials reported are referenced to an Fc/Fc^+ internal standard (set at + 0.6 V).

absorbance versus time (Figure S8, Supporting Information). Under ambient conditions (O_2 and H_2O present), no decomposition was observed for these FP end-capped DTTR-based compounds, demonstrating their good environmental stability for organic semiconductors.[23]

The FP end-capped DTTRs were also studied via DFT computations at the B3LYP/6-31G(d) level of theory to investigate the frontier molecular orbitals (FMOs) and energy minimized molecular geometries prior to further device characterization. The DFT-optimized lowest energy conformer of these two compounds and HOMO/LUMO contours are depicted in Figure S9 in the Supporting Information. Both molecules proved similar wave function delocalization over the whole conjugated backbone in their FMOs. FP terminal units do not significantly alter the density distribution of FMOs due to the large torsion (12.4–14.6°) angles between the capping moiety and π-spacers (T and bT). Compared to compound 1, compound 2 with a longer conjugated bridge (bithiophene) exhibits a significantly reduced HOMO–LUMO gap (3.08 vs 2.83 eV) with energetically destabilized HOMO and stabilized LUMO, consistent with the DPV results. The DFT calculation also shows that the center DTTR core and adjacent thiophene unit adopt the torsional angle of ≈40° for both compounds. However, the calculated geometries of compound 2 demonstrate the insertion of bithiophene units, enabling the whole molecule more twisted geometries and large steric hindrance for intrachain π-orbital delocalization, which is known to reduce the efficient charge transport.[61,63]

Thin films of compounds 1 and 2 were deposited by solution-shearing following the previously reported methodology.[51,64–65] The cover blade was held in place with the top vacuum stage and the (2-phenylethyl)trichlorosilane (PETS)-treated SiO_2/Si substrates were fixed to the bottom stage. The substrate stage was heated to the desired temperature. The compound 1 and 2 chlorobenzene solutions were confined to the meniscus-shaped gap formed by these two plates and the organic semiconductor crystalline films were fabricated onto the substrates as the cover blade moved along the substrate at a fixed speed. Thin film morphologies were characterized by polarized optical microscope (POM) and atomic force microscope (AFM). As seen in POM (**Figure 5**a), solution-sheared compound 1 film consists of aligned ribbon-like crystals, whereas compound 2 film exhibits discrete and small-sized crystals in fibers. Also, compound 1 crystals are of consistent color, potentially indicating the organized molecular packing inside the crystals. AFM images were captured using the taping mode with a scanning area of 20 × 20 μm (Figure 5b), featuring the same crystallite shapes obtained by POM. The long ribbon-like morphologies of compound 1 become distinctly oriented along the shearing direction, separated by pronounced boundaries. However, compound 2 films form discrete irregular domains that are randomly distributed, which displays the less crystalline features with much smaller aggregated domains from the morphology analysis. It was thus evident that to obtain the aligned ribbon-like domain, the π-spacer linkage is critical in the studied DTTR-based organic semiconductors system.

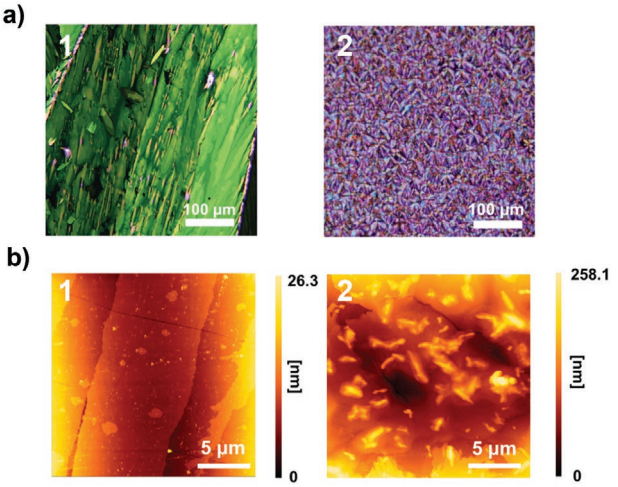

Figure 5. a) POM and b) AFM height images of solution-sheared compound 1 and 2 films.

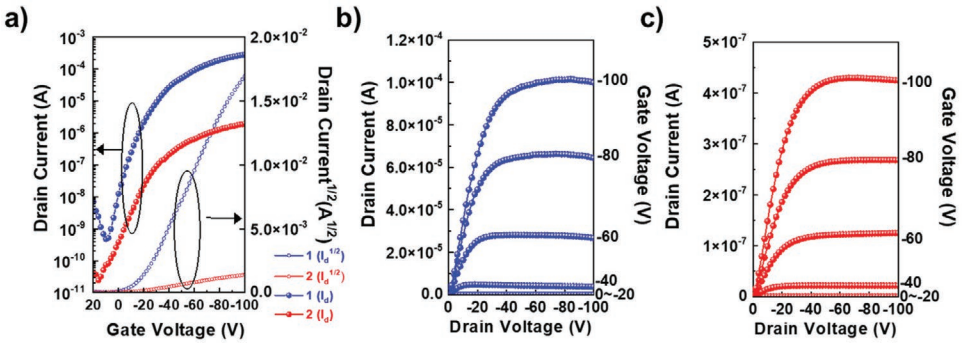

Figure 6. a) Transfer characteristics for compound 1 and 2 OFETs. Output characteristics for b) compound 1 and c) 2 OFETs.

The sheared organic semiconductor films were also used to fabricate the top-gate bottom-contact (TGBC) OFET devices to examine the charge transport properties. **Figure 6**a illustrates the transfer curves of both OFET devices based on solution-sheared film, measuring at a drain voltage (V_g) of –100 V and sweeping gate voltage range of 0 to –100 V. It should be noted that the channel direction of all tested OFETs is parallel to shearing direction. Representative semilogarithmic and square root plot of drain current (I_d) versus V_g are provided. A negative V_g modulates the charge carrier transfer demonstrating the prominent p-type behavior; hole transport metrics extracted from electrical characteristics are collected in **Table 2**. The output characteristics (I_d vs V_d at different negative V_g values; Figure 6b,c) indicated that all OFETs operated in the typical p-channel enhancement mode and exhibited the pinch-off with good current saturation. The slope and intercept of linear fits to the $I_d^{1/2}$–V_g data provide the fitting for field effect mobility and threshold voltage (V_{th}) when evaluated in the saturation region of OFET model. Compound 1 had better hole mobility with a maximum (μ_{max}) and average (μ_{avg}) at 0.48 and 0.23 ± 0.09 cm^2 V^{-1} s^{-1}, respectively, V_{th} of –25.8 ± 14.2 V with a good I_d modulation of 10^4–10^6. In contrast, compound 2 OFET exhibited μ_{max}/μ_{avg} of 1.82×10^{-3}/$(8.40 \pm 6.95) \times 10^{-4}$ cm^2 V^{-1} s^{-1}, threshold voltage (V_{th}) of –5.2 ± 8.2 V and ON/OFF current ratio (I_{ON}/I_{OFF}) of 10^2–10^4. The field effect mobility of compound 1 was around 300 times higher than that of compound 2 under dark conditions. Therefore, tailoring the π-conjugated moieties in linkage arms can modify the degree of steric hindrance and charge transport mobilities. We hypothesize that the poor electrical performance of compound 2 is related to the bithiophene spacer which disturbs the π–π stacking in the more twisted compound 2. In addition, a certain degree of non-linearity in the transfer characteristics ($I_d^{1/2}$–V_g curve) can be observed, and the channel mobility calculated shows that it increases slowly but up to a constant value when measured as function of V_g, as shown in Figure S10 in the Supporting Information. Therefore, the calculated measurement reliability factor (r) as well as effective mobility (μ_{eff}) are listed in Table 2 to prevent the mobility overestimation during the mobility extraction in our OFETs.[66–67] Although those re-estimated μ_{eff} values are slightly lower than μ_{max}, both trends in mobilities are consistent with compound 1 much higher than compound 2. Besides, both storage stability in ambient (relative humidity: 40–50%; room temperature) and operational stability under continuous electrical bias are provided in **Figure 7**. The extracted relative changes in mobility of both compound 1 and 2 over time (measured for 15 days, Figure 7a) exhibit the stable electrical properties of the unencapsulated device during storage in ambient. The measured transfer curves and the threshold voltage shift (ΔV_{th}) over stress time are given in Figure S11 in the Supporting Information and Figure 7b, respectively. Remarkably, compound 1 OFET undergoes a much lower ΔV_{th} than that observed for compound 2, which saturates at ΔV_{th} of ≈–10 V.

The crystallographic information from 2D grazing-incidence X-ray diffraction (GIXRD) was used to clarify the charge transport properties of the organic semiconductor films, as shown in **Figure 8**. These two compounds generate several distinct high order spots in the direction of q_z (out-of-plane), implying a highly crystalline structure. Note that the second- and fourth-order peaks of compound 1 are barely visible, possibly ascribed to the equal thickness of the two alternating layers of the lamellar packing that greatly reduces the scattering intensities of the even-order peaks.[68] The short diffraction arcs, especially for compound 1, observed throughout the pattern indicate a high degree of preferential orientation.[69] Both compound 1 and 2 diffraction patterns exhibit out-of-plane lamellar packing reflections identified starting at around 0.25 to 0.27 Å^{-1} and in-plane π–π reflection around 1.83 to 1.74 Å^{-1}, which corresponds to the lamellar stacking spacings of 25.1 and 23.4 Å, and π–π stacking distances of 3.4 and 3.6 Å, respectively. These results indicate that both compounds adopt an edge-on molecular packing in the crystal domains, with the linear alkyl side chains almost orthogonal to the substrate surface. Both the lamellar distances were longer than the theoretical length of the fully extended undecyl side chains (15.0 Å), implying these side chains arrange in an interdigitated manner. Despite an

Table 2. Summary of OFET devices characteristics based on solution-sheared compound 1 and 2 films.

Compound	μ_{max} [cm^2 V^{-1} s^{-1}]	μ_{avg} [cm^2 V^{-1} s^{-1}]	r [%]	μ_{eff} [cm^2 V^{-1} s^{-1}]	I_{ON}/I_{OFF} [–]	V_{th} [V]
DFPT-DTTR (1)	0.48	0.23 ± 0.09	27	0.13	10^4–10^6	–25.8 ± 14.2
DFPbT-DTTR (2)	1.82×10^{-3}	$(8.40 \pm 6.95) \times 10^{-4}$	29	5.28×10^{-4}	10^2–10^4	–5.2 ± 8.2

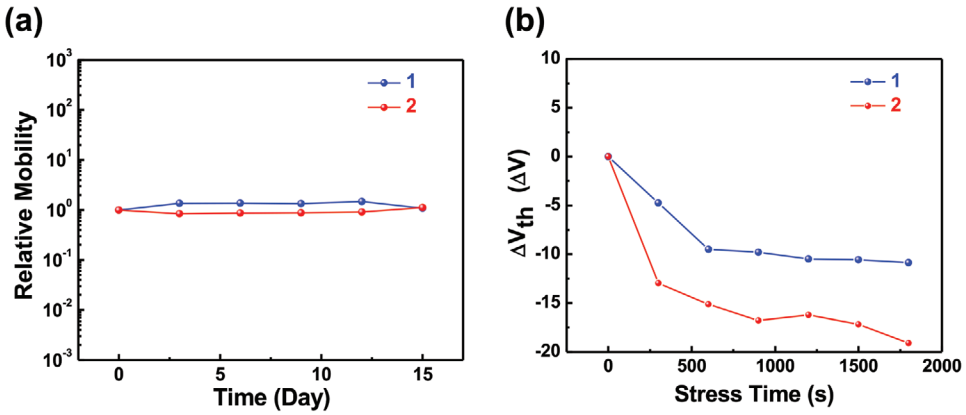

Figure 7. a) Relative mobility value of the OFETs after different storage times. b) The threshold voltage shift of the OFETs as a function of bias stress time.

analogous packing mode between these two compounds, the contrasting large compound 1 crystalline domains have shorter π–π distances as well as greater torsional rigidity. These may drive the macroscale aligned and connected compound 1 crystals in macroscale through the stronger π-stacking interaction even though the lower crystallinity of compound 1 (from the out-of-plane line cut profile of GIXRD; Figure S12, Supporting Information), resulting in the higher charge transport mobility.

3. Conclusion

In summary, two new alkylated DTTR-based small molecule analogs end-capped with FP units and bridged with thiophene and bithiophene rings were developed for solution-processed OFETs application. Variation of π-conjugated spacers is an effective structural modification strategy to manipulate the charge transport ability, demonstrated by compound 1 with a thiophene spacer having much higher mobility of 0.48 $cm^2\ V^{-1}\ s^{-1}$ with a high ON/OFF ratio of 10^4–10^6 compared to compound 2 with a bithiophene spacer (1.82×10^{-3} $cm^2\ V^{-1}\ s^{-1}$). The improved charge transport of compound 1 may be attributed to the less twisted molecular backbone, larger crystalline domains with better interconnected morphologies, and closer π–π stacking. Our studies reveal that the fused-ring connected alkylated DTTR central core with FP end-capping groups are important building blocks for solution-processed organic semiconductors and offer a better understanding of the effect of π-conjugated bridges on charge transport properties.

4. Experimental Section

General Procedures for Final Target Compounds (1–2): Details for the preparation of intermediates are provided in the Supporting Information. Under anhydrous and oxygen-free operating conditions, 2.5 M *n*-BuLi (0.84 mL in hexanes, 2.10 mmol) at –78 °C was slowly added to the intermediate 8 or 10 (0.92 mmol)/30 mL THF, then after reacting for 1 h, tri-*n*-butylstannyl chloride (2.10 mmol) was added dropwise at –78 °C, returned to room temperature and reacted for 12 h. Without purification, the THF was directly drained, and tetrakis-(triphenylphosphine)palladium (0.037 mmol)/20 mL toluene and 2-bromo-5-pentafluorophenylthiophene (2.1 mmol)/30 mL toluene were added to the reaction flask and reflux for two days. The reaction was terminated with the addition of water and the solid was filtered, rinsed with hexanes, and recrystallized from toluene to yield the final compound.

Synthesis of DFPT-DTTR (1): The title compound was obtained as an orange solid (yield = 55%). Mp: 169 °C. ^{1}H NMR (500 MHz, $CDCl_3$): δ 7.54 (d, J = 3.9 Hz, 2 H), 7.24 (d, J = 3.9 Hz, 2 H), 2.96 (t, J = 7.9 Hz, 4 H), 1.83–1.77 (m, 4 H), 1.37–1.25 (m, 32 H), 0.87 (t, J = 6.9 Hz, 6 H). ^{13}C NMR (125 MHz, $CDCl_3$): δ 145.17–145.02, 143.31, 143.21–143.00, 141.15–141.00, 139.46–139.40, 139.27–138.90, 137.37–137.11, 133.96, 130.71–130.62, 130.48, 129.09, 126.23, 109.99–109.71, 31.93, 29.67–29.01, 22.67, 14.01. ^{19}F NMR (282 MHz, $CDCl_3$): δ-139, –155, –161. MS (HR-MALDI, m/z) calcd. for $C_{50}H_{50}F_{10}S_5$: 1000.2356. Found: 1000.2351.

Synthesis of DFPbT-DTTR (2): The title compound was obtained as a red solid (yield = 67%). Mp: 165 °C. ^{1}H NMR (500 MHz, $CDCl_3$): δ 7.47 (d, J = 3.7 Hz, 2 H), 7.21 (d, J = 3.8 Hz, 2 H), 7.19 (d, J = 3.8 Hz, 2 H), 7.07 (d, J = 3.6 Hz, 2 H), 2.92 (t, J = 7.9 Hz, 4 H), 1.82-1.76 (m, 4 H), 1.37–1.26 (m, 32 H), 0.87 (t, J = 6.9 Hz, 6 H). ^{13}C NMR (125 MHz, $CDCl_3$): Insufficiently soluble to obtain a spectrum even at 55 °C. ^{19}F NMR (282 MHz, $CDCl_3$): δ-139, -155, -161. MS (HR-MALDI, m/z) calcd. for $C_{58}H_{54}F_{10}S_7$: 1164.2111. Found: 1164.2105.

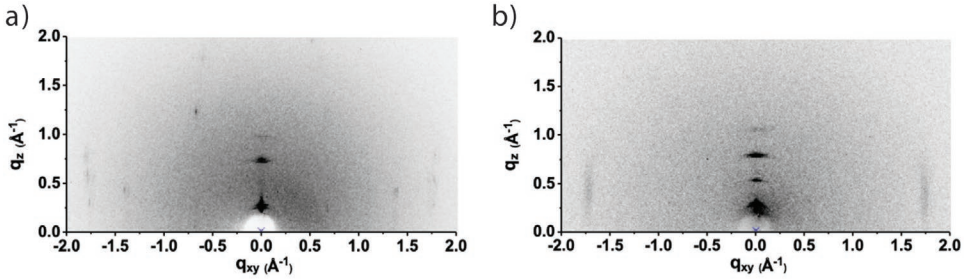

Figure 8. 2D scattering patterns for solution-sheared a) compound 1 and b) 2 films determined by GIXRD.

OFET Devices Fabrication and Characterization: The fabrication of OFETs was according to previous procedures,[51,64–65] using solution-shearing from 3 mg mL^{-1} 1 or 2 solutions dissolved in chlorobenzene at room temperature onto PETS-treated 300 nm SiO_2/Si substrates. A droplet (15 µL) of the solutions was injected into the gap between the upper coating blade and substrate at a deposition temperature of 60–90 °C on the heated stage where the pulling speed was maintained at 10–60 µm s^{-1}. The fabricated organic semiconductor films were then annealed at 80 °C overnight under vacuum and a top-contact 50 nm thick Au electrode was deposited through a shadow mask at a deposition rate of ≈1 Å s^{-1} and chamber pressure of 1×10^{-6} torr. The channel length (L) and width (W) were 25 and 1500 µm, respectively. The electrical characterization was measured at room temperature using a Keithley 4200-SCS semiconductor parameter analyzer inside the inert atmosphere of a nitrogen glove box. The measured transfer curves were analyzed to determine the OFET parameters, including filed effect mobility (μ), V_{th}, and current ON/OFF ratio (I_{ON}/I_{OFF}), using the general metal-oxide-semiconductor (MOS) transistor formula for a saturation region. The average parameters were calculated from more than ten independent device cells.

Supporting Information

Supporting Information is available from the Wiley Online Library or from the author.

Acknowledgements

A.V., Y.-C.Y., and C.-C.L. contributed equally to this work. The authors acknowledge the financial support received from the Ministry of Science and Technology (MOST) in Taiwan. M.-C. Chen thanks MOST (109-3111-8-008-001), MOST (110-2628-8-008-007) and NCU-Covestro Research Center. C.-L.L. acknowledges financial support from the Young Scholar Fellowship Program (Columbus Program) by MOST in Taiwan, under Grant MOST 110-2636-E-002-021. The authors also thank Beamline B13A1/B17A1/B23A1 at National Synchrotron Radiation Research Center (NSRRC) of Taiwan for providing beamtime.

Conflict of Interest

The authors declare no conflict of interest.

Data Availability Statement

Research data are not shared.

Keywords

dithienothiophene, organic semiconductors, organic transistor, perfluorophenyl, solution-processing

Received: June 24, 2021
Revised: October 22, 2021
Published online: November 16, 2021

[1] H. Bronstein, C. B. Nielsen, B. C. Schroeder, I. McCulloch, *Nat. Rev. Chem.* **2020**, *4*, 66.
[2] H. Chen, W. Zhang, M. Li, G. He, X. Guo, *Chem. Rev.* **2020**, *120*, 2879.
[3] Z. Lu, C. Wang, W. Deng, M. T. Achille, J. Jie, X. Zhang, *J. Mater. Chem. C* **2020**, *8*, 9133.
[4] S. Fratini, M. Nikolka, A. Salleo, G. Schweicher, H. Sirringhaus, *Nat. Mater.* **2020**, *19*, 491.
[5] Y. Wang, L. Sun, C. Wang, F. Yang, X. Ren, X. Zhang, H. Dong, W. Hu, *Chem. Soc. Rev.* **2019**, *48*, 1492.
[6] X. Gu, L. Shaw, K. Gu, M. F. Toney, Z. Bao, *Nat. Commun.* **2018**, *9*, 534.
[7] Y. Yu, Q. Ma, H. Ling, W. Li, R. Ju, L. Bian, N. Shi, Y. Qian, M. Yi, L. Xie, W. Huang, *Adv. Funct. Mater.* **2019**, *29*, 1904602.
[8] B. Kang, F. Ge, L. Qiu, K. Cho, *Adv. Electron. Mater.* **2017**, *3*, 1600240.
[9] B. Wang, W. Huang, L. Chi, M. Al-Hashimi, T. J. Marks, A. Facchetti, *Chem. Rev.* **2018**, *118*, 5690.
[10] G. Wang, F. S. Melkonyan, A. Facchetti, T. J. Marks, *Angew. Chem., Int. Ed.* **2019**, *58*, 4129.
[11] C. Yan, S. Barlow, Z. Wang, H. Yan, A. K. Y. Jen, S. R. Marder, X. Zhan, *Nat. Rev. Mater.* **2018**, *3*, 18003.
[12] S. Yuvaraja, A. Nawaz, Q. Liu, D. Dubal, S. G. Surya, K. N. Salama, P. Sonar, *Chem. Soc. Rev.* **2020**, *49*, 3423.
[13] Y. H. Lee, M. Jang, M. Y. Lee, O. Y. Kweon, J. H. Oh, *Chem* **2017**, *3*, 724.
[14] K. Takimiya, S. Shinamura, I. Osaka, E. Miyazaki, *Adv. Mater.* **2011**, *23*, 4347.
[15] Y. Pan, G. Yu, *Chem. Mater.* **2021**, *33*, 2229.
[16] D. J. Gundlach, J. E. Royer, S. K. Park, S. Subramanian, O. D. Jurchescu, B. H. Hamadani, A. J. Moad, R. J. Kline, L. C. Teague, O. Kirillov, C. A. Richter, J. G. Kushmerick, L. J. Richter, S. R. Parkin, T. N. Jackson, J. E. Anthony, *Nat. Mater.* **2008**, *7*, 216.
[17] Q. Miao, M. Lefenfeld, T.-Q. Nguyen, T. Siegrist, C. Kloc, C. Nuckolls, *Adv. Mater.* **2005**, *17*, 407.
[18] K. Ito, T. Suzuki, Y. Sakamoto, D. Kubota, Y. Inoue, F. Sato, S. Tokito, *Angew. Chem., Int. Ed.* **2003**, *42*, 1159.
[19] T.-H. Chao, M.-J. Chang, M. Watanabe, M.-H. Luo, Y. J. Chang, T.-C. Fang, K.-Y. Chen, T. J. Chow, *Chem. Commun.* **2012**, *48*, 6148.
[20] J. E. Anthony, J. S. Brooks, D. L. Eaton, S. R. Parkin, *J. Am. Chem. Soc.* **2001**, *123*, 9482.
[21] S. Vegiraju, D.-Y. Huang, P. Priyanka, Y.-S. Li, X.-L. Luo, S.-H. Hong, J.-S. Ni, S.-H. Tung, C.-L. Wang, W.-C. Lien, S. L. Yau, C.-L. Liu, M.-C. Chen, *Chem. Commun.* **2017**, *53*, 5898.
[22] L. Wang, J. Dai, Y. Song, *Int. J. Quantum Chem.* **2019**, *119*, e25824.
[23] C. Kim, P.-Y. Huang, J.-W. Jhuang, M.-C. Chen, J.-C. Ho, T.-S. Hu, J.-Y. Yan, L.-H. Chen, G.-H. Lee, A. Facchetti, T. J. Marks, *Org. Electron.* **2010**, *11*, 1363.
[24] J. Youn, P.-Y. Huang, Y.-W. Huang, M.-C. Chen, Y.-J. Lin, H. Huang, R. P. Ortiz, C. Stern, M.-C. Chung, C.-Y. Feng, L.-H. Chen, A. Facchetti, T. J. Marks, *Adv. Funct. Mater.* **2012**, *22*, 48.
[25] J. Youn, S. Vegiraju, J. D. Emery, B. J. Leever, S. Kewalramani, S. J. Lou, S. Zhang, K. Prabakaran, Y. Ezhumalai, C. Kim, P.-Y. Huang, C. Stern, W.-C. Chang, M. J. Bedzyk, L. X. Chen, M.-C. Chen, A. Facchetti, T. J. Marks, *Adv. Electron. Mater.* **2015**, *1*, 1500098.
[26] C. Zhang, X. Zhu, *Adv. Funct. Mater.* **2020**, *30*, 2000765.
[27] Y. Sun, Y. Guo, Y. Liu, *Mater. Sci. Eng., R* **2019**, *136*, 13.
[28] C. Wang, H. Dong, W. Hu, Y. Liu, D. Zhu, *Chem. Rev.* **2012**, *112*, 2208.
[29] Z. Xue, S. Chen, N. Gao, Y. Xue, B. Lu, O. A. Watson, L. Zang, J. Xu, *Polym. Rev.* **2020**, *60*, 318.
[30] S. N. Afraj, G.-Y. He, C.-Y. Lin, A. Velusamy, C.-Y. Huang, P.-S. Lin, S. Vegiraju, P.-Y. Huang, J.-S. Ni, S.-L. Yau, S.-H. Tung, T. Minari, C.-L. Liu, M.-C. Chen, *Adv. Mater. Technol.* **2021**, *6*, 2001028.
[31] M.-C. Chen, S. Vegiraju, C.-M. Huang, P.-Y. Huang, K. Prabakaran, S. L. Yau, W.-C. Chen, W.-T. Peng, I. Chao, C. Kim, Y.-T. Tao, *J. Mater. Chem. C* **2014**, *2*, 8892.
[32] N. C. Mamillapalli, S. Vegiraju, P. Priyanka, C.-Y. Lin, X.-L. Luo, H.-C. Tsai, S.-H. Hong, J.-S. Ni, W.-C. Lien, G. Kwon, S. L. Yau, C. Kim, C.-L. Liu, M.-C. Chen, *Dyes Pigm.* **2017**, *145*, 584.
[33] M. Kim, S. U. Ryu, S. A. Park, K. Choi, T. Kim, D. Chung, T. Park, *Adv. Funct. Mater.* **2020**, *30*, 1904545.

[34] K. Takimiya, I. Osaka, T. Mori, M. Nakano, *Acc. Chem. Res.* **2014**, *47*, 1493.
[35] S. Vegiraju, A. A. Amelenan Torimtubun, P.-S. Lin, H.-C. Tsai, W.-C. Lien, C.-S. Chen, G.-Y. He, C.-Y. Lin, D. Zheng, Y.-F. Huang, Y.-C. Wu, S.-L. Yau, G.-H. Lee, S.-H. Tung, C.-L. Wang, C.-L. Liu, M.-C. Chen, A. Facchetti, *ACS Appl. Mater. Interfaces* **2020**, *12*, 25081.
[36] K. Xiao, Y. Liu, T. Qi, W. Zhang, F. Wang, J. Gao, W. Qiu, Y. Ma, G. Cui, S. Chen, X. Zhan, G. Yu, J. Qin, W. Hu, D. Zhu, *J. Am. Chem. Soc.* **2005**, *127*, 13281.
[37] X.-C. Li, H. Sirringhaus, F. Garnier, A. B. Holmes, S. C. Moratti, N. Feeder, W. Clegg, S. J. Teat, R. H. Friend, *J. Am. Chem. Soc.* **1998**, *120*, 2206.
[38] Y. Liu, Y. Wang, W. Wu, Y. Liu, H. Xi, L. Wang, W. Qiu, K. Lu, C. Du, G. Yu, *Adv. Funct. Mater.* **2009**, *19*, 772.
[39] Y. Liu, C.-a. Di, C. Du, Y. Liu, K. Lu, W. Qiu, G. Yu, *Chem. - Eur. J.* **2010**, *16*, 2231.
[40] Y. M. Sun, Y. Q. Ma, Y. Q. Liu, Y. Y. Lin, Z. Y. Wang, Y. Wang, C. A. Di, K. Xiao, X. M. Chen, W. F. Qiu, B. Zhang, G. Yu, W. P. Hu, D. B. Zhu, *Adv. Funct. Mater.* **2006**, *16*, 426.
[41] M.-C. Chen, Y.-J. Chiang, C. Kim, Y.-J. Guo, S.-Y. Chen, Y.-J. Liang, Y.-W. Huang, T.-S. Hu, G.-H. Lee, A. Facchetti, T. J. Marks, *Chem. Commun.* **2009**, 1846.
[42] C. Kim, M.-C. Chen, Y.-J. Chiang, Y.-J. Guo, J. Youn, H. Huang, Y.-J. Liang, Y.-J. Lin, Y.-W. Huang, T.-S. Hu, G.-H. Lee, A. Facchetti, T. J. Marks, *Org. Electron.* **2010**, *11*, 801.
[43] H. Usta, D. Kim, R. Ozdemir, Y. Zorlu, S. Kim, M. C. Ruiz Delgado, A. Harbuzaru, S. Kim, G. Demirel, J. Hong, Y.-G. Ha, K. Cho, A. Facchetti, M.-G. Kim, *Chem. Mater.* **2019**, *31*, 5254.
[44] M.-C. Chen, C. Kim, S.-Y. Chen, Y.-J. Chiang, M.-C. Chung, A. Facchetti, T. J. Marks, *J. Mater. Chem.* **2008**, *18*, 1029.
[45] T. J. Marks, *MRS Bull.* **2010**, *35*, 1018.
[46] H. Usta, C. Risko, Z. Wang, H. Huang, M. K. Deliomeroglu, A. Zhukhovitskiy, A. Facchetti, T. J. Marks, *J. Am. Chem. Soc.* **2009**, *131*, 5586.
[47] S. Vegiraju, G.-Y. He, C. Kim, P. Priyanka, Y.-J. Chiu, C.-W. Liu, C.-Y. Huang, J.-S. Ni, Y.-W. Wu, Z. Chen, G.-H. Lee, S.-H. Tung, C.-L. Liu, M.-C. Chen, A. Facchetti, *Adv. Funct. Mater.* **2017**, *27*, 1606761.
[48] A. Velusamy, C.-H. Yu, S. N. Afraj, C.-C. Lin, W.-Y. Lo, C.-J. Yeh, Y.-W. Wu, H.-C. Hsieh, J. Chen, G.-H. Lee, S.-H. Tung, C.-L. Liu, M.-C. Chen, A. Facchetti, *Adv. Sci.* **2021**, *8*, 2002930.
[49] Y. Yang, Z. Liu, G. Zhang, X. Zhang, D. Zhang, *Adv. Mater.* **2019**, *31*, 1903104.
[50] N. Zhou, S. Vegiraju, X. Yu, E. F. Manley, M. R. Butler, M. J. Leonardi, P. Guo, W. Zhao, Y. Hu, K. Prabakaran, R. P. H. Chang, M. A. Ratner, L. X. Chen, A. Facchetti, M.-C. Chen, T. J. Marks, *J. Mater. Chem. C* **2015**, *3*, 8932.
[51] S. Vegiraju, X.-L. Luo, L.-H. Li, S. N. Afraj, C. Lee, D. Zheng, H.-C. Hsieh, C.-C. Lin, S.-H. Hong, H.-C. Tsai, G.-H. Lee, S.-H. Tung, C.-L. Liu, M.-C. Chen, A. Facchetti, *Chem. Mater.* **2020**, *32*, 1422.
[52] C.-C. Lin, S. N. Afraj, A. Velusamy, P.-C. Yu, C.-H. Cho, J. Chen, Y.-H. Li, G.-H. Lee, S.-H. Tung, C.-L. Liu, M.-C. Chen, A. Facchetti, *ACS Nano* **2021**, *15*, 727.
[53] T. Dong, L. Lv, L. Feng, Y. Xia, W. Deng, P. Ye, B. Yang, S. Ding, A. Facchetti, H. Dong, H. Huang, *Adv. Mater.* **2017**, *29*, 1606025.
[54] H. Huang, L. Yang, A. Facchetti, T. J. Marks, *Chem. Rev.* **2017**, *117*, 10291.
[55] V. Joseph, C.-H. Yu, C.-C. Lin, W.-C. Lien, H.-C. Tsai, C.-S. Chen, A. A. A. Torimtubun, A. Velusamy, P.-Y. Huang, G.-H. Lee, S.-L. Yau, S.-H. Tung, T. Minari, C.-L. Liu, M.-C. Chen, *J. Mater. Chem. C* **2020**, *8*, 15450.
[56] A. Facchetti, M.-H. Yoon, C. L. Stern, H. E. Katz, T. J. Marks, *Angew. Chem., Int. Ed.* **2003**, *42*, 3900.
[57] J. A. Letizia, A. Facchetti, C. L. Stern, M. A. Ratner, T. J. Marks, *J. Am. Chem. Soc.* **2005**, *127*, 13476.
[58] M.-H. Yoon, S. A. DiBenedetto, A. Facchetti, T. J. Marks, *J. Am. Chem. Soc.* **2005**, *127*, 1348.
[59] M.-H. Yoon, C. Kim, A. Facchetti, T. J. Marks, *J. Am. Chem. Soc.* **2006**, *128*, 12851.
[60] J. S. Reddy, T. Kale, G. Balaji, A. Chandrasekaran, S. Thayumanavan, *J. Phys. Chem. Lett.* **2011**, *2*, 648.
[61] S. J. Cho, M. J. Kim, Z. Wu, J. H. Son, S. Y. Jeong, S. Lee, J. H. Cho, H. Y. Woo, *ACS Appl. Mater. Interfaces* **2020**, *12*, 41842.
[62] J. Youn, M.-C. Chen, Y.-j. Liang, H. Huang, R. P. Ortiz, C. Kim, C. Stern, T.-S. Hu, L.-H. Chen, J.-Y. Yan, A. Facchetti, T. J. Marks, *Chem. Mater.* **2010**, *22*, 5031.
[63] X. Gong, C. Zheng, X. Feng, Y. Huan, J. Li, M. Yi, Z. Fu, W. Huang, D. Gao, *Chem. - Asian J.* **2018**, *13*, 3920.
[64] S. Vegiraju, B.-C. Chang, P. Priyanka, D.-Y. Huang, K.-Y. Wu, L.-H. Li, W.-C. Chang, Y.-Y. Lai, S.-H. Hong, B.-C. Yu, C.-L. Wang, W.-J. Chang, C.-L. Liu, M.-C. Chen, A. Facchetti, *Adv. Mater.* **2017**, *29*, 1702414.
[65] S. Vegiraju, C.-Y. Lin, P. Priyanka, D.-Y. Huang, X.-L. Luo, H.-C. Tsai, S.-H. Hong, C.-J. Yeh, W.-C. Lien, C.-L. Wang, S.-H. Tung, C.-L. Liu, M.-C. Chen, A. Facchetti, *Adv. Funct. Mater.* **2018**, *28*, 1801025.
[66] C. Liu, G. Li, R. Di Pietro, J. Huang, Y.-Y. Noh, X. Liu, T. Minari, *Phys. Rev. Appl.* **2017**, *8*, 034020.
[67] H. H. Choi, K. Cho, C. D. Frisbie, H. Sirringhaus, V. Podzorov, *Nat. Mater.* **2018**, *17*, 2.
[68] T.-Y. Lai, C.-Y. Cheng, W.-Y. Cheng, K.-M. Lee, S.-H. Tung, *Macromolecules* **2015**, *48*, 717.
[69] J. Rivnay, S. C. B. Mannsfeld, C. E. Miller, A. Salleo, M. F. Toney, *Chem. Rev.* **2012**, *112*, 5488.